

# Infrared-Faint Radio Sources are at high redshifts

## Spectroscopic redshift determination of Infrared-Faint Radio Sources using the Very Large Telescope

A. Herzog<sup>1,2,3</sup>, E. Middelberg<sup>1</sup>, R. P. Norris<sup>3,4</sup>, R. Sharp<sup>5</sup>, and L. R. Spitler<sup>2,6</sup>

<sup>1</sup> Astronomisches Institut, Ruhr-Universität Bochum, Universitätsstr. 150, 44801 Bochum, Germany  
e-mail: herzog@astro.rub.de

<sup>2</sup> Macquarie University, Sydney, NSW 2109, Australia

<sup>3</sup> CSIRO Astronomy and Space Science, Marsfield, PO Box 76, Epping, NSW 1710, Australia

<sup>4</sup> ARC Centre of Excellence for All-sky Astrophysics (CAASTRO)

<sup>5</sup> Research School of Astronomy & Astrophysics, Australian National University, Mount Stromlo Observatory, Cotter road, Weston Creek, ACT 2611, Australia

<sup>6</sup> Australian Astronomical Observatory, PO Box 915, North Ryde, NSW 1670, Australia

Received Month xx, 2013; accepted Month xx, 2013

### ABSTRACT

**Context.** Infrared-Faint Radio Sources (IFRS) are characterised by relatively high radio flux densities and associated faint or even absent infrared and optical counterparts. The resulting extremely high radio-to-infrared flux density ratios up to several thousands were previously known only for High-redshift Radio Galaxies (HzRGs), suggesting a link between these classes of object. However, the optical and infrared faintness of IFRS makes their study difficult. So far, no redshift is known for an original IFRS which would help to put IFRS in the context of other classes of object, especially of HzRGs.

**Aims.** This work tests the hypothesis that IFRS follow the relation between  $3.6 \mu\text{m}$  flux density and redshift found for HzRGs. Furthermore, redshifts will enable us to reveal the intrinsic radio and infrared properties of IFRS and we will test the current suggestions that IFRS are high-redshift radio-loud active galactic nuclei.

**Methods.** A sample of IFRS was spectroscopically observed using the Focal Reducer and low dispersion Spectrograph 2 (FOR2) at the Very Large Telescope (VLT). The data are reduced based on the Image Reduction and Analysis Facility (IRAF) and redshifts extracted from the final spectra, where possible. This required information is then used to calculate rest-frame luminosities and to perform the first spectral energy distribution modelling based on redshifts.

**Results.** We find three IFRS to be located at redshifts of 1.84, 2.13, and 2.76, confirming the high-redshift character of this class of object. High-ionisation emission lines with high equivalent widths and modelling of the spectral energy distribution support the hypothesis that IFRS contain radio-loud active galactic nuclei. We find IFRS being similar to HzRGs and especially observe IFRS to follow the relation between  $3.6 \mu\text{m}$  flux density and redshift found for HzRGs.

**Key words.** Techniques: spectroscopic – Galaxies: active – Galaxies: distances and redshifts – Galaxies: high-redshift

## 1. Introduction

Active Galactic Nuclei (AGN) at high redshifts are an important field of current research since they take a key role in answering basic questions about the evolution of the universe. For example, high-redshift AGN are used to study the evolution of the link between black hole mass and the properties of its host galaxy (e.g., Hopkins et al. 2005, Lamastra et al. 2010), their impact on the reionisation and the structure formation in the universe (e.g., Fan et al. 2006, Robertson et al. 2010, Boutsia et al. 2011) and the growth of supermassive black holes (SMBHs) with masses  $> 10^9 M_\odot$  in less than one billion years after the Big Bang (e.g., Volonteri & Rees 2005). Infrared-Faint Radio Sources (IFRS) – a class of object whose detection was very surprising – could significantly contribute to the population of high-redshift AGN. When Norris et al. (2006) crossmatched the deep 1.4 GHz radio maps from the Australia Telescope Large Area Survey (ATLAS) with the data from the *Spitzer* Wide-area Infrared Extragalactic Survey (SWIRE; Lonsdale et al. 2003), it was expected that SWIRE would provide an infrared (IR) counterpart for any ex-

tragalactic radio source detected in ATLAS, regardless whether the radio emission is produced by AGN or starforming activity. However, 22 sources without an IR counterpart ( $3\sigma = 3 \mu\text{Jy}$  at  $3.6 \mu\text{m}$ ) were found in Chandra Deep Field South (CDF2). These sources were labeled as IFRS. Using the same approach, Middelberg et al. (2008a) identified 31 IFRS using ATLAS radio observations of the European Large Area ISO survey South 1 (ELAIS-S1) field and SWIRE data. In total, 53 IFRS were detected in ATLAS, showing 1.4 GHz flux densities between tenths and tens of mJy.

The first attempts to further characterise the properties of IFRS used Very Long Baseline Interferometry (VLBI) observations. Norris et al. (2007) observed two IFRS and identified an AGN in one of them, showing a linear size of  $\leq 260$  pc at any redshift. Furthermore, Middelberg et al. (2008b) detected one of four targeted IFRS with VLBI and derived a brightness temperature of  $3.6 \times 10^6$  K, implying non-thermal emission from an AGN since thermal emission processes cannot produce such high temperatures. Therefore, Middelberg et al. concluded that at least a fraction of all IFRS contain AGN.

Garn & Alexander (2008) found a sample of 14 IFRS in the *Spitzer* First Look Survey (FLS) field, using *Spitzer* Infrared Array Camera (IRAC; Fazio et al. 2004) and Multiband Imaging Photometer (MIPS; Rieke et al. 2004) data. They concluded from spectral energy distribution (SED) modelling that IFRS are probably 3C sources redshifted to  $2 \leq z \leq 5$ . Moreover, they excluded obscured starforming galaxies (SFGs) as an explanation for the objects in their sample because of the radio-to-IR flux density ratio upper limits, differing significantly from corresponding values of SFGs.

The first SED modelling of ATLAS-IFRS was presented by Huynh et al. (2010), using new ultra-deep imaging in the extended CDFS (eCDFS). From their detailed SED modelling of four IFRS, Huynh et al. concluded that a 3C 273-like object can reproduce the data when redshifted to  $z = 2$  in case of an IR detection or redshifted to  $z = 4$  in case of an IR non-detection. Furthermore, they stated that no SED template can explain an IR non-detection at  $z < 4$ . According to Garn & Alexander (2008), Huynh et al. showed that all four analysed IFRS fall well beyond the radio-IR correlation, suggesting the radio emission is produced by the presence of an AGN, but not by starforming activity.

Middelberg et al. (2011) studied the radio properties of 17 IFRS from the ATLAS ELAIS-S1 sample between 2.3 and 8.4 GHz. They found a median radio spectral index of  $\alpha = -1.4^1$  and no index larger than  $-0.7$  which is significantly steeper compared to the radio spectra of the general source population as well as of the AGN source population in the ATLAS ELAIS-S1 field. Additionally, Middelberg et al. noticed several similarities between IFRS and the sample of High-redshift Radio Galaxies (HzRGs) from Seymour et al. (2007), showing a median radio spectral index of  $-1.02$ . Moreover, the extremely high radio-to-IR flux density ratios of IFRS overlap with those of this HzRG sample. The hypothesis of an AGN content in at least a fraction of all IFRS was supported by Middelberg et al. who identified ten IFRS of their sample as AGN and the other seven as most likely AGN.

These similarities between IFRS and HzRGs were emphasised by Norris et al. (2011) who showed that no other type of object occupies the range of radio-to-IR flux density ratios of IFRS except for HzRGs. The sample of HzRGs of Seymour et al. (2007) shows a relation between the  $3.6 \mu\text{m}$  flux density and redshift similar to the  $K - z$  relation for other radio galaxies (Willott et al. 2003). If IFRS also follow this relation, they would all be placed at  $z \geq 2$ , reaching redshifts of 5. Furthermore, Norris et al. used deep data from the *Spitzer* Extragalactic Representative Volume Survey (SERVS; Mauduit et al. 2012) with a  $3\sigma$  noise level of  $\sim 1.5 \mu\text{Jy}$  at  $3.6 \mu\text{m}$  in the fields of CDFS and ELAIS-S1 and stacked the  $3.6 \mu\text{m}$  images of 39 IFRS, resulting in a flux density upper limit of  $\sim 0.2 \mu\text{Jy}$ , emphasising the significant IR faintness of IFRS.

Since the selection criterion for IFRS – a radio source showing no IR counterpart – was survey-specific, Zinn et al. (2011) introduced two survey-independent selection criteria for the identification of IFRS:

- (i) a radio-to-IR flux density ratio  $S_{20 \text{ cm}}/S_{3.6 \mu\text{m}} > 500$  and
- (ii) a  $3.6 \mu\text{m}$  flux density  $S_{3.6 \mu\text{m}} < 30 \mu\text{Jy}$ .

Applying these criteria, Zinn et al. compiled a catalog of 55 IFRS in four deep radio fields (CDFS, ELAIS-S1, FLS, and COSMOS) and derived a survey-independent IFRS sky density of  $(30.8 \pm 15.0) \text{ deg}^{-2}$ .

<sup>1</sup> The spectral index is defined as  $S \sim \nu^\alpha$ .

Recently, Maini et al. (in prep.) found 21 IFRS in the Lockman Hole and looked for IR counterparts of IFRS located in the SERVS deep fields. Collier et al. (2013) used data from the all-sky survey Wide-Field Infrared Survey Explorer (WISE; Wright et al. 2010) and the Unified Radio Catalog (URC; Kimball & Ivezić, in prep.) and presented a catalogue of 1317 IFRS which fulfill the selection criteria from Zinn et al. (2011) but are much brighter than the IFRS found in the ATLAS fields. Collier et al. suggested that their IFRS are closer versions of the IFRS found by Norris et al. (2006) and Middelberg et al. (2008a).

All observational findings so far suggest the majority if not all IFRS to be high-redshift ( $z > 2$ ) radio-loud AGN, perhaps suffering from heavy dust extinction. Considering their high sky density, IFRS could be a very numerous and so far overlooked population of high-redshift AGN, probably with significant impact on the evolution of the universe as suggested by Zinn et al. (2011). Furthermore, Zinn et al. concluded that the X-ray emission of AGN-driven IFRS is consistent with the unresolved components of the Cosmic X-ray background reported by Moretti et al. (2003).

In this paper, we present the first redshifts of IFRS in the ATLAS field based on spectroscopic observations made using the Focal Reducer and low dispersion Spectrograph 2 (FOR2; Appenzeller et al. 1998) on the Very Large Telescope (VLT). Using these results we test the hypothesis that IFRS follow the  $S_{3.6 \mu\text{m}} - z$  relation of HzRGs, derive intrinsic properties of IFRS, compare them to other objects and model the SEDs of IFRS. The sample of observed IFRS and the VLT FOR2 observations are described in Sect. 2. In Sect. 3, we summarise the data reduction and calibration and show the final spectra. In Sect. 4, redshifts are measured and intrinsic properties derived for our sample of IFRS. We test our hypotheses in Sect. 5 and present our conclusions in Sect. 6. The cosmological parameters used in this paper are  $\Omega_\Lambda = 0.7$ ,  $\Omega_M = 0.3$ ,  $H_0 = 70 \text{ km s}^{-1} \text{ Mpc}^{-1}$  in combination with the web-based calculator by Wright (2006). We present IR luminosities in the form  $\nu L_\nu/L_\odot$ , where  $L_\odot = 3.9 \times 10^{26} \text{ W}$ , and radio luminosities as luminosity densities, following common practice.

## 2. Sample and observations

The sample of IFRS consists of four objects, chosen by their detected optical counterparts between 22.0 and 24.1 (Vega) magnitudes in the  $R$  band. This implies that these sources were originally not considered as IFRS by Norris et al. (2006) but fulfill the two criteria by Zinn et al. (2011) mentioned in Sect. 1. The condition of an optical counterpart ensures that the sources are bright enough for optical spectroscopy. However, this biases the observed sample towards less extreme IFRS, i.e. showing a faint optical counterpart and providing radio-to-IR flux density ratios between 600 and 1100. Most known IFRS do not show an optical counterpart and, therefore, are not suitable for optical spectroscopy. Although the observed sample is not representative of all IFRS, it allows us to gather information about the intrinsic properties of less extreme IFRS and test the hypotheses about their relation to other classes of object. Further, these findings will also allow conclusions on the more extreme IFRS which cannot be achieved by spectroscopy because of their deep optical and IR faintness. We summarise the observed objects and their characteristic properties in Table 1.

The longslit spectroscopic observations of these IFRS were carried out in project 087.B-0813(A) between July and September 2011 (ESO Period 87) in service mode, using FOR2 on UT1 at the VLT. Using the GRISM\_150I grism and a slit width

**Table 1.** Sample of spectroscopically observed IFRS. Listed is the ID, the position in RA and DEC, the radio flux density at 1.4 GHz, the IR flux density at 3.6  $\mu\text{m}$ , the radio-to-IR flux density ratio between 1.4 GHz and 3.6  $\mu\text{m}$ , the optical  $R$  band (Vega) magnitude, the on-source time and the redshift determined in this work. Positions, flux densities and magnitudes are taken from Norris et al. (2006).

IFRS ID	RA J2000.0	DEC	$S_{1.4\text{ GHz}}$ [mJy]	$S_{3.6\ \mu\text{m}}$ [ $\mu\text{Jy}$ ]	$S_{1.4\text{ GHz}}/S_{3.6\ \mu\text{m}}$	$R$ (Vega) [mag]	$t_{\text{obs}}$ [min]	$z$
S212	03:29:48.942	-27:31:48.98	18.9	17.5	1080	22.0	44	$2.76 \pm 0.05$
S265	03:30:34.661	-28:27:06.51	18.6	29.3	635	22.3	88	$1.84 \pm 0.03$
S539	03:33:30.542	-28:54:28.22	9.1	14.2	641	24.1	45	–
S713	03:35:37.525	-27:50:57.88	16.4	25.5	643	22.4	128	$2.13 \pm 0.03$

of 2'', a high throughput is achieved at the cost of relatively low resolution, although sufficient to provide reliable redshifts. The dispersion is 3.45 Å/pixel, resulting in a resolution of 54.76 Å. The total on-source time are 44 min for S212, 88 min for S265, 45 min for S539 and 128 min for S713, where the exposure time for each object was split into several shorter exposures, enabling the correction of cosmic ray events. The seeing varied during and between the different observations from 0.86'' to 2.46''.

### 3. Data reduction and calibration

Data reduction is carried out using the standard Image Reduction and Analysis Facility (IRAF) procedures. All exposures are bias-corrected and flatfielded, where we use a normalised masterflat, basing on the individual dome flat exposures, whose faulty pixels are previously corrected using a bad pixel mask. We reject some single flat field exposures before creating the masterflat where an imperfect illumination is obvious. Cosmic rays are removed using the IRAF task `cosmicrays` and manual inspection. Since the objects are not located in exactly one line in the two-dimensional spectra, i.e. the spatial position changes as a function of wavelength, we correct the spatial axis for this distortion. Consequently, the wavelength calibration is carried out using lamp exposures taken in every observing night. Since all lamp exposures are saturated and the determination of the lines' peak positions is impossible, we apply a block average with width 3 on the spectral axis to all exposures used in the entire reduction procedure. After applying the wavelength calibration, we subtract the sky background using the IRAF task `background`. Finally, all individual exposures of one object are averaged to increase the signal-to-noise ratio and we extract the one-dimensional spectra by applying a suitable aperture at the object's position using the IRAF task `apall`. For IFRS S265 which was observed on 2011-Jul-16 and 2011-Jul-30, we use only the data taken on 2011-Jul-30 for the final spectrum due to the bad quality of the data taken on 2011-Jul-16, arising from seeing in the range of 2.5'' compared to 0.9'' on the other day. The resulting one- and two-dimensional spectra of IFRS S212, S265, S713, and S539 are shown in Fig. 1.

### 4. Redshifts and intrinsic properties of IFRS

Using the one-dimensional spectra, we measure redshifts – where applicable – from the Mg II line which is generally considered to be the most reliable high ionisation line. Where Mg II is not available, we use C IV to derive the redshift, although C IV is known to be systematically different from the galaxy's redshift (Isaak et al. 2002; Priddey et al. 2007). However, we do not find any offset in our low-resolution spectra.

Since the calibration uncertainty in the spectra is negligible compared to the uncertainty in the determination of the line position, we derive the redshift uncertainty only from the uncertainty in

the line position which is obtained from a Gaussian fit to the emission line. We note that all redshifts measured from all available emission lines listed in Table 2 are within the uncertainty of our best redshift measured from Mg II or C IV.

Using the obtained redshifts, we calculate K-corrected radio luminosities, assuming a power law  $S \sim \nu^\alpha$  with a radio spectral index of  $-1.4$  which is the median spectral index found by Middelberg et al. (2011) for a sample of 17 IFRS from the ATLAS sample. For the calculation of the K-corrected 3.6  $\mu\text{m}$  IR luminosities, we use a spectral index of 0.7 between 5.8 and 24  $\mu\text{m}$ , deduced from Fig. 2 in Lacy et al. (2004). They show an IRAC-MIPS 24  $\mu\text{m}$  color-color plot, including a sample of obscured AGN. Since we measure redshifts between 1.84 and 2.76 for our IFRS, their observed 3.6  $\mu\text{m}$  fluxes are emitted at rest wavelengths around 10 to 15  $\mu\text{m}$ . Therefore, the spectral index in the rest-frame wavelength range between 5.8 and 24  $\mu\text{m}$  is most suitable to calculate K-corrected 3.6  $\mu\text{m}$  luminosities.

#### 4.1. S212

Three broad emission lines with FWHM between 78 and 169 Å are visible in the spectrum of S212 which we identify as Ly $\alpha$ , C IV, and C III], at a redshift  $z = 2.76 \pm 0.05$  (see Fig. 1, upper left). Furthermore, a less distinct emission line can be associated with Si IV at around 5260 Å. The broad emission lines of a few thousand  $\text{km s}^{-1}$  suggest the presence of an AGN in S212. Using the determined redshift and the measured flux densities listed in Table 1, S212 has a 1.4 GHz luminosity of  $2.0 \times 10^{27} \text{ W Hz}^{-1}$  and a 3.6  $\mu\text{m}$  luminosity of  $2.5 \times 10^{10} L_{\odot}$ .

#### 4.2. S265

We find three broad emission lines with FWHM between 57 and 223 Å in the spectrum of S265 in Fig. 1 (upper right) which we identify as C IV, C III], and Mg II, at a redshift  $z = 1.84 \pm 0.03$ . These broad emission lines with line widths in the range of 4000 to 8000  $\text{km s}^{-1}$  clearly suggest the presence of an AGN in S265. We find a 1.4 GHz luminosity of  $6.7 \times 10^{26} \text{ W Hz}^{-1}$  and a 3.6  $\mu\text{m}$  luminosity of  $2.5 \times 10^{10} L_{\odot}$ .

#### 4.3. S713

Three broad emission lines are visible in the spectrum of S713, showing FWHM between 88 and 134 Å, corresponding to line widths about 5000  $\text{km s}^{-1}$  and suggesting the presence of an AGN. The lines are associated to C IV, C III], and Mg II at a redshift  $z = 2.13 \pm 0.03$  (see Fig. 1, lower left). We find a 1.4 GHz luminosity of  $8.7 \times 10^{26} \text{ W Hz}^{-1}$  and a 3.6  $\mu\text{m}$  luminosity of  $2.6 \times 10^{10} L_{\odot}$ .

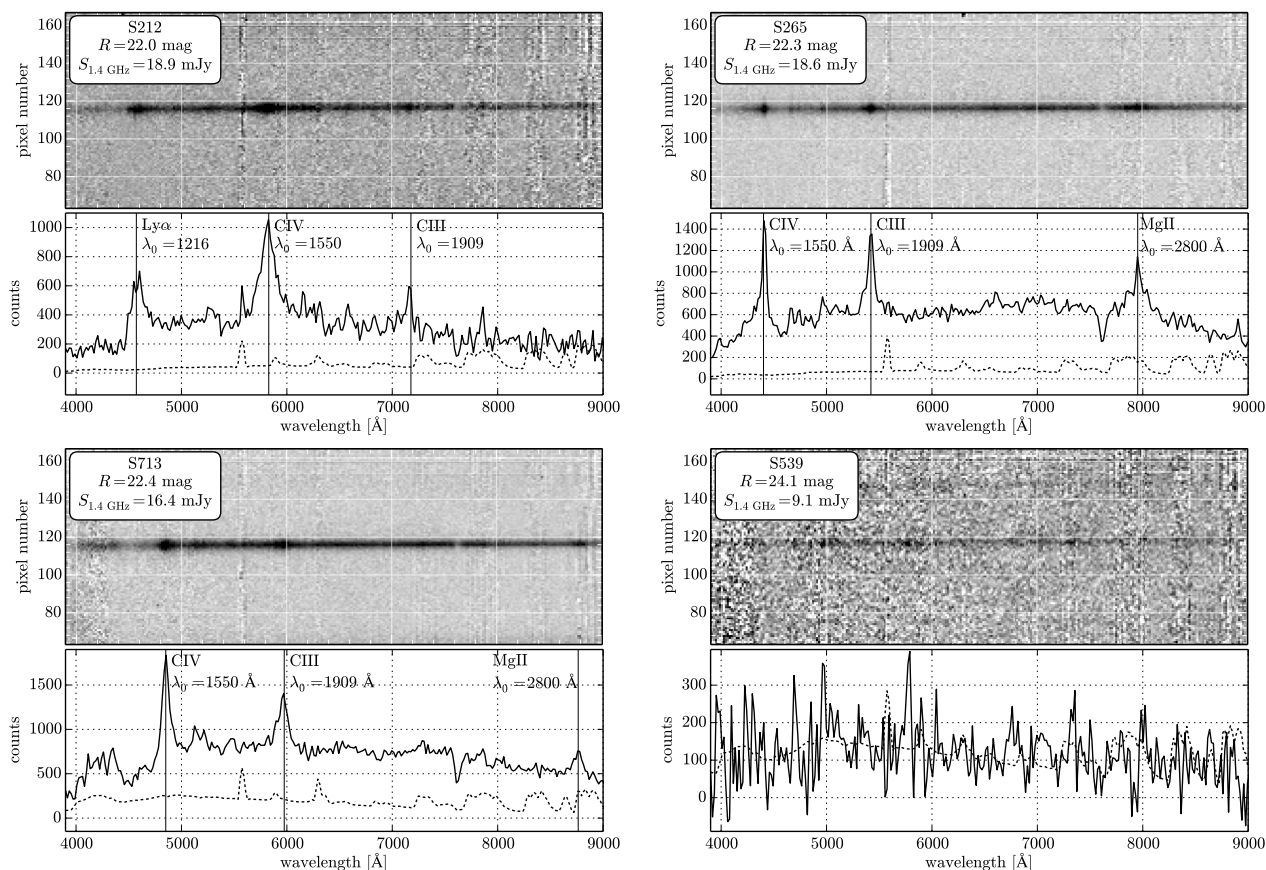


**Fig. 1.** Spectra of IFRS S212 (upper left), S265 (upper right), S713 (lower left), and S539 (lower right). For each IFRS we show the two-dimensional (upper image) and the extracted one-dimensional (lower plot) spectrum. We list the ID, the  $R$  band magnitude and the 1.4 GHz radio flux density of each IFRS. In the one-dimensional spectrum, the solid line represents the spectrum of the IFRS while the dotted line shows the sky background in arbitrary units. Additionally, the position of emission lines are marked by vertical lines for a redshift of  $z = 2.76$  (S212),  $z = 1.84$  (S265), and  $z = 2.13$  (S713), respectively.

**Table 2.** Spectroscopic information of the four IFRS observed with FORS2. Listed is the IFRS ID, the spectroscopic redshift and the emission line identified in the spectrum with the associated line width. We obtain the final redshift of each IFRS from the Mg II emission line and from C IV where Mg II is not available.

IFRS ID	$z$	Line	FWHM [km s <sup>-1</sup> ]
S212	$2.76 \pm 0.05$	C IV	$8700 \pm 600$
	$2.75 \pm 0.02$	C III	$3300 \pm 700$
S265	$1.85 \pm 0.02$	C IV	$3900 \pm 500$
	$1.84 \pm 0.02$	C III	$4200 \pm 300$
S713	$1.84 \pm 0.03$	Mg II	$8400 \pm 900$
	$2.13 \pm 0.03$	C IV	$5400 \pm 700$
	$2.12 \pm 0.03$	C III	$5900 \pm 400$
S539	–	–	–

#### 4.4. S539

IFRS S539 is the optically faintest object in this observing programme. However, it was only observed for 44 min on-source time, although an observing time of 3 h was proposed. Therefore, the resulting spectrum does not provide the quality of the other spectra and we cannot use it to measure redshift and line widths (see Fig. 1, lower right). Despite the short integration time, emis-

sion features are visible, however at a very poor signal-to-noise ratio. We expect the emission feature at around 4970 Å to be Ly $\alpha$ , indicated by the related break towards lower wavelengths and a second emission feature at redder wavelengths which we expect to be Si IV. We suggest S539 to be at redshift  $z \sim 3.1$ , although the low signal-to-noise ratio prevents a reliable statement.

## 5. Discussion

We have shown that the redshifts of the IFRS in our sample lie between 1.8 and 2.8. This result is in agreement with the conclusions of Garn & Alexander (2008), Huynh et al. (2010), Norris et al. (2011) and Zinn et al. (2011) who suggested IFRS to be located at redshifts above 2, mainly from SED modelling. As mentioned in Sect. 2, we were aware that the selection of the optically brightest IFRS might bias our sample towards lower redshifts. This seems to be confirmed by the deduced redshifts which are in the lower part of the expected range  $2 < z < 5$  for IFRS. Recently, Collier et al. (2013) presented 19 IFRS with spectroscopic redshifts. Their sample is extracted from a shallow all-sky survey, in contrast to the IFRS analysed in this paper which are found in the deep ATLAS field. Therefore, the IFRS found by Collier et al. are brighter than the ones presented in this work and might be a less extreme population of IFRS. Nevertheless, Collier et al. find redshifts in the range  $2 < z < 3$  in

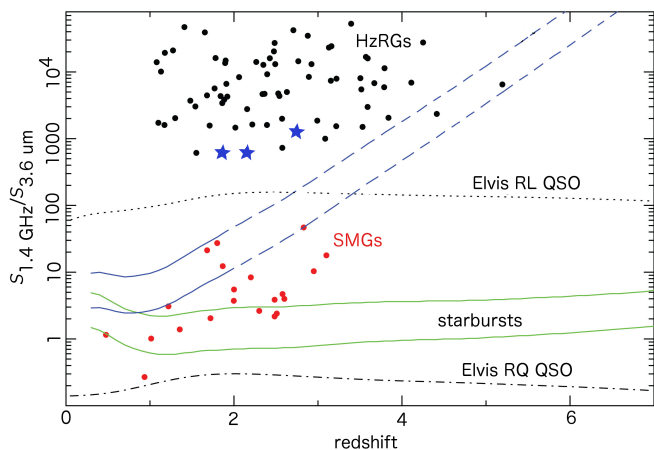


**Fig. 2.** Ratio of 1.4 GHz and  $3.6 \mu\text{m}$  flux densities for IFRS and several other classes of object as a function of redshift, adapted from Norris et al. (2011). It shows that the IFRS analysed in this paper (blue stars) are more similar to HzRGs (black dots, Seymour et al. 2007) than to other types of galaxies which are frequently found at high redshifts. The solid lines indicate the expected loci of luminous and ultra-luminous infrared galaxies (ULIRGs), using the templates from Rieke et al. (2009). The dotted and dot-dashed lines indicate the loci of a classical radio-loud and radio-quiet QSO, respectively, from Elvis et al. (1994). The location of classical sub-millimetre galaxies is indicated by the red dots. We note that dust extinction could cause any of the calculated tracks to rise steeply at high redshift, where the observed  $3.6 \mu\text{m}$  emission is generated in visible wavelengths in the galaxy rest frame. This is illustrated by the dashed lines which show the effect of adding  $A_v = 8^m$  of extinction to the two starburst tracks. However, the radio emission from these galaxies would be undetectable at  $z > 2$  with current sensitivity.

agreement with the redshifts obtained in this work.

All spectra shown in Fig. 1 are broad-line quasar spectra, characterised by high-ionisation emission lines with high equivalent widths. This finding agrees with former suggestions by Garn & Alexander (2008), Huynh et al. (2010), Norris et al. (2011) and Zinn et al. (2011) that IFRS contain AGN.

IFRS are characterised by their extremely high radio-to-IR flux density ratios typically in the range of several hundreds to a few thousands. The redshifts determined in Sect. 4 enable us to put these three IFRS in the plot showing the radio-to-IR flux density versus redshift (Fig. 2). This plot clearly separates IFRS from other classes of object which are typically found at high redshifts and indicates a potential connection between IFRS and HzRGs. Norris et al. (2011) suggested that IFRS might follow a relation between redshift and  $3.6 \mu\text{m}$  flux density, similar to the correlation found for the sample of HzRGs by Seymour et al. (2007). This paper primarily attempts to test this hypothesis. Figure 3 shows the  $3.6 \mu\text{m}$  IR flux density versus redshift for the three IFRS whose redshifts we determined in Sect. 4. We find these IFRS following the relationship suggested by Norris et al., providing evidence that these objects are HzRGs. We emphasise that the IFRS analysed in this paper are the optically and IR-brightest IFRS as described in Sect. 2. We expect that IFRS with no detected IR counterpart may have redshifts as high as 5 or 6. Moreover, the availability of redshifts allows us for the first time to perform a more accurate SED fitting. Garn & Alexander (2008), Huynh et al. (2010) and Zinn et al. (2011) modelled SEDs to constrain the redshift of IFRS. Here, in contrast, we can use the redshift as an anchor and use it to test different SED templates against available photometric data.

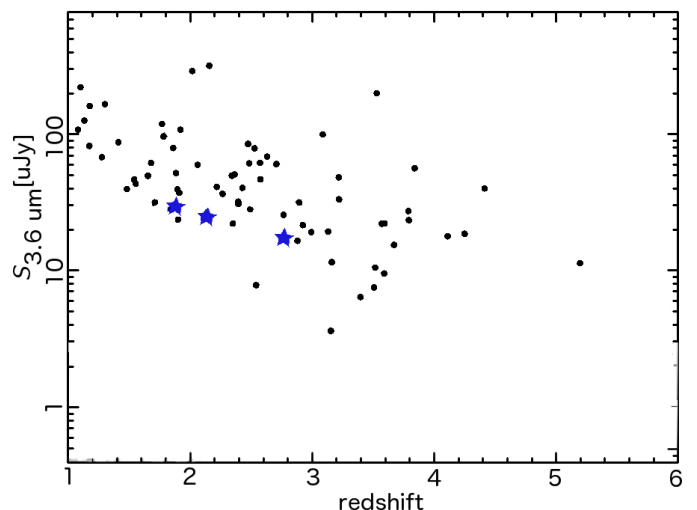


**Fig. 3.**  $3.6 \mu\text{m}$  IR flux density versus redshift, adapted from Norris et al. (2011). Shown is the sample of HzRGs from Seymour et al. (2007) as black dots and the three IFRS whose redshifts are presented in this work as blue stars. The IFRS are located in the same parameter range as the HzRGs and follow their  $S_{3.6 \mu\text{m}} - z$  relation.

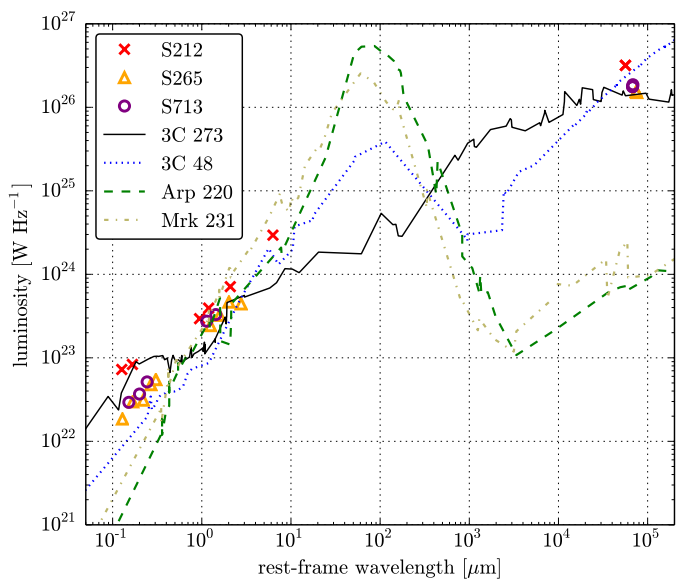


**Fig. 4.** Rest-frame SED fitting for the three IFRS whose redshifts are determined in this work. All templates are shifted to the rest-frame and scaled in luminosity to match the photometric datapoints shown by red crosses (S212), orange triangles (S265) and purple circles (S713). While the SED templates of starforming galaxy Arp 220 (green dashed line) and Seyfert galaxy Mrk 231 (olive dashed-dotted line) clearly disagree with the available photometric data, the templates of the radio-loud quasar 3C 273 (black solid line) and the compact steep spectrum (CSS) source 3C 48 (blue dotted line) fulfill the requirements.

We build the SED templates using photometric data and redshifts from the NASA/IPAC Extragalactic Database (NED), connecting the datapoints by lines and smoothing the template. We use a variety of SED templates, including starburst, radio and dwarf galaxies as well as quasars. Furthermore, we take all available photometric data of the IFRS from Norris et al. (2006). These data consist of optical ( $G$  and  $R$  bands), IR ( $3.6$  and  $4.5 \mu\text{m}$ ) and

**Table 3.** Luminosities of the objects considered in this work. We list the luminosity at  $3.6 \mu\text{m}$ , the FIR luminosity as an indicator for the bolometric luminosity, and the 1.4 GHz luminosity for the three IFRS, as well as for 3C 273, 3C 48, and HzRGs.

source	$L_{3.6 \mu\text{m}}$ [ $L_{\odot}$ ]	$L_{\text{FIR}}$ [ $L_{\odot}$ ]	$L_{1.4 \text{ GHz}}$ [ $\text{W Hz}^{-1}$ ]
S212	$2.5 \times 10^{10}$	$10^{11}$	$2.0 \times 10^{27}$
S265	$2.5 \times 10^{10}$	$4 \times 10^{10}$	$6.7 \times 10^{26}$
S713	$2.6 \times 10^{10}$	$4 \times 10^{10}$	$8.7 \times 10^{26}$
3C 273	$2.5 \times 10^{12}$	$6.3 \times 10^{11}$	$3.1 \times 10^{27}$
3C 48	$5.9 \times 10^{11}$	$4.0 \times 10^{12}$	$6.8 \times 10^{27}$
HzRGs	$> 4 \times 10^{10}$	$> 10^{12}$	$> 1.8 \times 10^{26}$

radio (1.4 GHz) flux densities for all three IFRS, while S212 and S265 provide more data points in the optical and IR range.

To model the IFRS’s SEDs, we shift the template SEDs to the rest-frame and scale them in luminosity to match the observed  $3.6 \mu\text{m}$  flux density of the IFRS. Extinction is added in the rest-frame optical and near-IR, following a Calzetti et al. (2000) reddening law, where required by the photometric data. Furthermore, all available photometric datapoints of the IFRS from NED are also shifted to the IFRS’s rest-frames and used to test the template SEDs for compatibility with these available constraints.

Figure 4 shows the SED fitting for the three IFRS. We find S265 and S713 have very similar SEDs. S212 is also similar, except that it is a factor of 2 or 3 brighter than the other two at all wavelengths. These SEDs are consistent with either the 3C 273 or the 3C 48 templates, with no reddening necessary, if the templates are scaled by a wavelength-independent factor 0.06 and 0.10, respectively. However, none of the other templates matches the SEDs of the IFRS, even with reddening applied.

This result confirms that IFRS are high-redshift radio-loud AGN. Our SED modelling is inconsistent with the alternative interpretation of IFRS mentioned by Norris et al. (2011), explaining IFRS as AGN suffering from heavy dust extinction.

In Sect. 4 we derived 1.4 GHz radio luminosities between  $6.7 \times 10^{26}$  and  $2.0 \times 10^{27} \text{ W Hz}^{-1}$  for the IFRS investigated in this work. The classical separation between Fanaroff & Riley (1974) type 1 and 2 is  $4.8 \times 10^{25}$  ( $1.7 \times 10^{25}$ )  $\text{W Hz}^{-1}$  at 1.4 GHz, using a steep (ultrasteep) radio spectral index  $\alpha = -0.8$  ( $-1.3$ ) for the conversion from the 178 MHz luminosity given by Fanaroff & Riley. This clearly classifies IFRS as Fanaroff & Riley type 2.

Seymour et al. (2007) defined an HzRG as a radio galaxy with  $z > 1$  and a 3 GHz luminosity above  $10^{26} \text{ W Hz}^{-1}$ , corresponding to  $1.8 \times 10^{26}$  ( $2.7 \times 10^{26}$ )  $\text{W Hz}^{-1}$  at 1.4 GHz (see Table 3 also in the following). We find the IFRS in agreement with the radio luminosity range of HzRGs, supporting the hypothesis mentioned by Norris et al. (2011) that IFRS might be siblings of HzRGs. We note that most IFRS are radio-brighter and possibly more radio-luminous than those analysed in this work.

We found  $3.6 \mu\text{m}$  IR rest-frame luminosities of around  $2.5 \times 10^{10} L_{\odot}$  for the IFRS whose redshifts are determined in this paper. HzRGs show mid-IR luminosities in the range of  $10^{10.5}$  to  $10^{12.5} L_{\odot}$  (Seymour et al. 2007, Fig. 10), showing the IFRS in the IR in agreement with the luminosities of HzRGs. Figure 3 in De Breuck et al. (2010) shows the rest-frame IR luminosity density versus wavelength for the sample of HzRGs defined by Seymour et al. and illustrates that the IFRS presented here complement the HzRG sample at lower IR luminosities.

Furthermore, we compare the IFRS with the luminosities of 3C 273 and 3C 48 which are the objects most suitable for mod-

elling the SEDs of IFRS as shown in this work. The radio-loud quasar 3C 273 shows a rest-frame radio luminosity of  $3.1 \times 10^{27} \text{ W Hz}^{-1}$  at 1.4 GHz, assuming a radio spectral index of  $-0.8$ . We find a corresponding luminosity for the compact steep spectrum (CSS) source 3C 48 of  $6.8 \times 10^{27} \text{ W Hz}^{-1}$ . The IFRS analysed in this paper show rest-frame 1.4 GHz luminosities which are up to one order of magnitude lower. We find a larger difference of up to two orders of magnitude between the rest-frame  $3.6 \mu\text{m}$  luminosities. The IFRS show values of  $2.5 \times 10^{10} L_{\odot}$ , whereas 3C 273 and 3C 48 have rest-frame  $3.6 \mu\text{m}$  luminosities of  $2.5 \times 10^{12} L_{\odot}$  and  $5.9 \times 10^{11} L_{\odot}$ , respectively.

We calculate the far-IR (FIR) luminosity from the 60 and 100  $\mu\text{m}$  flux densities, following Helou et al. (1988). Using data from NED, we obtain a FIR luminosity of  $6.3 \times 10^{11} L_{\odot}$  for 3C 273 and  $4.0 \times 10^{12} L_{\odot}$  for 3C 48. Based on the results from our SED modelling, we assume the shape of the IFRS’s SED to be given by 3C 273 (3C 48). We use the scaling factor of 0.06 (0.10) found in the fitting to match the photometric constraints and obtain FIR luminosities of  $4 \times 10^{10}$  ( $4 \times 10^{11}$ )  $L_{\odot}$ . We note that a higher FIR luminosity is expected for IFRS S212 because of its higher intrinsic brightness (see Fig. 4). We take these FIR luminosities as a rough estimate of the bolometric luminosities since the bolometric luminosity of starforming galaxies is usually dominated by the FIR luminosity.

In this work, we confirm the high redshifts of IFRS which were suggested by Garn & Alexander (2008) Huynh et al. (2010), Norris et al. (2011) and Zinn et al. (2011) mainly from SED modelling. Furthermore, we find evidence that IFRS are radio-loud quasars which is in agreement with prior suggestions. Our results show that IFRS are similar to HzRGs (Seymour et al. 2007) with respect to redshifts and luminosities, as suggested by Middelberg et al. (2011) and Norris et al. (2011). The IFRS analysed in this paper are the optically and IR brightest IFRS in the ATLAS field. We find evidence that IFRS follow the correlation between  $3.6 \mu\text{m}$  flux density and redshift which implies that the optically and IR fainter IFRS could easily be located at redshifts of 5 or 6. Considering the high sky density of IFRS in the range of a few per square degree, there is evidence that the class of IFRS represents an enormous number of quasars.

Zinn et al. (2011) showed that IFRS have a significant impact on structure formation and the growth of galaxies in the early universe, assuming that IFRS are at high redshifts and contain an AGN. In the present work, we find strong evidence that most if not all IFRS are such high-redshift AGN, pointing at the cosmological relevance of IFRS. Furthermore, our results indicate that IFRS follow the correlation between  $3.6 \mu\text{m}$  flux density and redshift as suggested by Norris et al. (2011). This relation would be an easy tool to find more and higher-redshift versions of this cosmologically non-negligible class of object.

## 6. Conclusions

We present the first spectroscopic data of four IFRS in the ATLAS field from the VLT FOR2 and specify the properties of IFRS.

- We determine the first redshifts of ATLAS IFRS and find three IFRS at  $z = 1.84, 2.13,$  and  $2.76$ , confirming the suggested high redshifts of IFRS.
- Broad emission lines with line widths between 3300 and 8700  $\text{\AA}$  found in all spectra confirm that IFRS contain AGN.
- Using the redshifts measured in this work, we present the first SED modelling of IFRS based on redshifts and find the template SEDs of radio-loud quasars to agree with that of IFRS.

- IFRS have derived radio and IR luminosities similar to those of HzRGs, providing further evidence for the similarity of IFRS and HzRGs.
- We test the hypothesis that IFRS follow the same correlation between  $3.6 \mu\text{m}$  flux density and redshift as HzRGs. Our findings support this hypothesis and support the suggestions that IFRS are related to HzRGs and might be fainter or higher-redshift siblings. The evidence found for the correlation between IR flux density and redshifts suggests that IR-fainter IFRS are at higher redshifts than those analysed in this paper.

*Acknowledgements.* We thank Peter-Christian Zinn for providing the basics of the code for the SED fitting. Based on observations made with ESO Telescopes at the La Silla Paranal Observatory under programme ID 087.B-0813(A). IRAF is distributed by the National Optical Astronomy Observatory, which is operated by the Association of Universities for Research in Astronomy (AURA) under cooperative agreement with the National Science Foundation. This research has made use of the NASA/IPAC Extragalactic Database (NED) which is operated by the Jet Propulsion Laboratory, California Institute of Technology, under contract with the National Aeronautics and Space Administration.

## References

- Appenzeller, I., Fricke, K., Fürtig, W., et al. 1998, *The Messenger*, 94, 1
- Boutsia, K., Grazian, A., Giallongo, E., et al. 2011, *ApJ*, 736, 41
- Calzetti, D., Armus, L., Bohlin, R. C., et al. 2000, *ApJ*, 533, 682
- Collier, J. D., Banfield, J. K., Norris, R. P., et al. 2013, submitted
- De Breuck, C., Seymour, N., Stern, D., et al. 2010, *ApJ*, 725, 36
- Elvis, M., Wilkes, B. J., McDowell, J. C., et al. 1994, *ApJS*, 95, 1
- Fan, X., Strauss, M. A., Becker, R. H., et al. 2006, *AJ*, 132, 117
- Fanaroff, B. L. & Riley, J. M. 1974, *MNRAS*, 167, 31P
- Fazio, G. G., Hora, J. L., Allen, L. E., et al. 2004, *ApJS*, 154, 10
- Garn, T. & Alexander, P. 2008, *MNRAS*, 391, 1000
- Helou, G., Khan, I. R., Malek, L., & Boehmer, L. 1988, *ApJS*, 68, 151
- Hopkins, P. F., Hernquist, L., Martini, P., et al. 2005, *ApJ*, 625, L71
- Huyh, M. T., Norris, R. P., Siana, B., & Middelberg, E. 2010, *ApJ*, 710, 698
- Isaak, K. G., Priddey, R. S., McMahon, R. G., et al. 2002, *MNRAS*, 329, 149
- Lacy, M., Storrie-Lombardi, L. J., Sajina, A., et al. 2004, *ApJS*, 154, 166
- Lamastra, A., Menci, N., Maiolino, R., Fiore, F., & Merloni, A. 2010, *MNRAS*, 405, 29
- Lonsdale, C. J., Smith, H. E., Rowan-Robinson, M., et al. 2003, *PASP*, 115, 897
- Mauduit, J.-C., Lacy, M., Farrah, D., et al. 2012, *PASP*, 124, 714
- Middelberg, E., Norris, R. P., Cornwell, T. J., et al. 2008a, *AJ*, 135, 1276
- Middelberg, E., Norris, R. P., Hales, C. A., et al. 2011, *A&A*, 526, A8
- Middelberg, E., Norris, R. P., Tingay, S., et al. 2008b, *A&A*, 491, 435
- Moretti, A., Campana, S., Lazzati, D., & Tagliaferri, G. 2003, *ApJ*, 588, 696
- Norris, R. P., Afonso, J., Appleton, P. N., et al. 2006, *AJ*, 132, 2409
- Norris, R. P., Afonso, J., Cava, A., et al. 2011, *ApJ*, 736, 55
- Norris, R. P., Tingay, S., Phillips, C., et al. 2007, *MNRAS*, 378, 1434
- Priddey, R. S., Gallagher, S. C., Isaak, K. G., et al. 2007, *MNRAS*, 374, 867
- Rieke, G. H., Alonso-Herrero, A., Weiner, B. J., et al. 2009, *ApJ*, 692, 556
- Rieke, G. H., Young, E. T., Engelbracht, C. W., et al. 2004, *ApJS*, 154, 25
- Robertson, B. E., Ellis, R. S., Dunlop, J. S., McLure, R. J., & Stark, D. P. 2010, *Nature*, 468, 49
- Seymour, N., Stern, D., De Breuck, C., et al. 2007, *ApJS*, 171, 353
- Volonteri, M. & Rees, M. J. 2005, *ApJ*, 633, 624
- Willott, C. J., Rawlings, S., Jarvis, M. J., & Blundell, K. M. 2003, *MNRAS*, 339, 173
- Wright, E. L. 2006, *PASP*, 118, 1711
- Wright, E. L., Eisenhardt, P. R. M., Mainzer, A. K., et al. 2010, *AJ*, 140, 1868
- Zinn, P.-C., Middelberg, E., & Ibar, E. 2011, *A&A*, 531, A14